Journal of Quantitative Spectroscopy & Radiative Transfer 254 (2020) 107202

Contents lists available at ScienceDirect

Journal of Quantitative Spectroscopy & Radiative Transfer

journal homepage: www.elsevier.com/locate/jqsrt

New infrared absorption cross sections for the infrared limb sounding of sulfur hexafluoride (SF_6)

Jeremy J. Harrison[a,b,c]

[a] Department of Physics and Astronomy, University of Leicester, University Road, Leicester LE1 7RH, United Kingdom
[b] National Centre for Earth Observation, University of Leicester, Leicester, LE1 7RH, United Kingdom
[c] Leicester Institute for Space and Earth Observation, University of Leicester, Leicester, LE1 7RH, United Kingdom

ARTICLE INFO

Article history:
Received 29 May 2020
Revised 6 July 2020
Accepted 6 July 2020
Available online 7 July 2020

Keywords:
SF_6
Sulfur hexafluoride
High-resolution fourier transform spectroscopy
Infrared absorption cross sections
Atmospheric remote sensing
Greenhouse gas

ABSTRACT

Sulfur hexafluoride (SF_6), widely used in industry for electrical insulation, is a potent greenhouse gas with a steadily increasing atmospheric abundance. In order to monitor its concentration profiles using infrared sounders, accurate laboratory spectroscopic data are required. This work describes new high-resolution infrared absorption cross sections of pure and air-broadened sulfur hexafluoride over the spectral range 780 – 1100 cm^{-1}, derived from spectra recorded using a high-resolution Fourier transform spectrometer (Bruker IFS 125HR) and a 26-cm-pathlength cell. Spectra were recorded at resolutions between 0.002 and 0.03 cm^{-1} (calculated as 0.9/MOPD; MOPD = maximum optical path difference) over a range of atmospherically relevant temperatures (189 – 294 K) and pressures (up to 751 Torr). These new absorption cross sections improve upon those previously used for remote sensing, and will provide a more accurate basis for retrievals in the future.

1. Introduction

With a global warming potential (GWP) of 23,500 over a hundred year time horizon, sulfur hexafluoride (SF_6) is the most potent greenhouse gas that has been evaluated by the Intergovernmental Panel on Climate Change (IPCC) [1]. On account of its strong electronegativity, high thermal conductivity, and thermal and chemical stability, SF_6 is widely used in industry as an insulating medium in high-voltage electrical equipment, in particular in electricity distribution systems, magnesium production, and semi-conductor manufacturing. Associated with these industrial applications, large amounts of SF_6 have leaked into the atmosphere. While the majority of SF_6 emissions are anthropogenic, there is believed to be a small natural source arising from the degassing of rocks, responsible for a background level of up to 0.01 ppt [2]. According to the latest WMO ozone assessment report in 2018 [3], the volume mixing ratio of SF_6 has increased in the atmosphere relatively rapidly by 3.90 ± 0.06% yr^{-1} (relative to 2013) between 2010 and 2016, where it reached a value of 8.9 ppt.

The atmospheric lifetime of SF_6 listed in recent IPCC and WMO reports is 3200 years [4], however recent studies suggest this value needs to be significantly revised downwards. Kovacs et al. [5] determined an average lifetime of 1278 (1120–1475) years using the Whole Atmosphere Community Climate Model (WACCM) and a more detailed treatment of electron attachment, which plays a major role in the atmospheric removal of SF_6. Ray et al. [6] estimated a lifetime of 850 (580–1400) years from in situ measurements of SF_6 in the 2000 Arctic polar vortex.

Measurements of sulfur hexafluoride in the stratosphere are used to derive mean age of air values, from which it is possible to investigate changes in the Brewer–Dobson circulation (BDC), the global circulation in the stratosphere. In a changing climate, it is particularly important to monitor the BDC as circulation changes could affect stratospheric ozone and the lifetimes of ozone-depleting substances [7]. General circulation and chemistry-climate models predict the BDC will speed up under climate change, however this has not yet been observed [7].

SF_6 can be measured by atmospheric limb sounders, for example by the satellite instruments ACE-FTS (Atmospheric Chemistry Experiment – Fourier transform spectrometer) [8], which has been measuring since 2004, and MIPAS (Michelson Interferometer for Passive Atmospheric Sounding) [7], which measured between 2002 and 2012. The ν_3 band of SF_6 at 948.1 cm^{-1} [9] is very intense with well resolved Q-band structure, and can be observed in atmospheric limb spectra despite its low abundance. As will be elaborated on in Section 2, the HITRAN SF_6 spectroscopic linelist is not currently recommended for use in remote-sensing applica-

E-mail address: jh592@leicester.ac.uk

https://doi.org/10.1016/j.jqsrt.2020.107202

tions because it is missing a number of hot bands. Instead it is recommended that HITRAN users utilise the HITRAN SF_6 absorption cross-section dataset, derived from measurements by Varanasi et al. [10,11]. However, even this HITRAN cross-section dataset has deficiencies, which will be fully addressed in Section 4. The purpose of the present work is to detail new pure and air-broadened SF_6 absorption cross sections which will provide a more accurate basis for the atmospheric remote sensing of SF_6.

2. Infrared spectroscopy of sulfur hexafluoride

Sulfur hexafluoride, an octahedral molecule with seven atoms and six fundamental vibrational modes (15 degrees of freedom overall), belongs to the O_h point group. Since fluorine has only one stable, naturally occurring isotope, ^{19}F, the natural abundances of SF_6 isotopologues follow those of the stable sulfur isotopes, i.e. $^{32}SF_6$ (95.02%), $^{33}SF_6$ (0.75%), $^{34}SF_6$ (4.21%), and $^{36}SF_6$ (0.02%). The six modes of SF_6 can be classified according to their symmetry: the three stretching modes ν_1 (A_{1g}, ~774.5 cm^{-1}), ν_2 (E_g, ~643.3 cm^{-1}) and ν_3 (F_{1u}, ~948.1 cm^{-1}), and the three bending modes ν_4 (F_{1u}, ~615.0 cm^{-1}), ν_5 (F_{2g}, ~524.0 cm^{-1}) and ν_6 (F_{2u}, ~347.7 cm^{-1}); wavenumbers in parentheses correspond to the $^{32}SF_6$ isotopologue [9]. Only ν_3 and ν_4 are formally infrared active, with ν_3 being the more strongly absorbing and the band of choice for atmospheric remote sensing. Fig. 1 gives an overview of the ν_3 band for the most abundant $^{32}SF_6$ isotopologue, along with the minor $^{33}SF_6$ and $^{34}SF_6$ isotopologues, for one of the new absorption cross sections at 189.4 K and 7.50 Torr. Details on the measurement conditions and derivation of this cross section are given in Section 3.

Line parameters for the strong ν_3 band of $^{32}SF_6$ at 948.1 cm^{-1} first appeared in the HITRAN 1991 compilation [12]. Although these were unchanged for the HITRAN 1996 compilation [13], it was pointed out that the linelist did not include parameters for the underlying hot bands, which contribute about half of the total absorption under stratospheric conditions. Users were strongly advised to instead adopt the recently added air-broadened SF_6 absorption cross sections of Varanasi over the spectral range 925–955 cm^{-1}, of which there were seven pressure-temperature (PT) combinations covering 216–295 K and 25–760 Torr. For the HITRAN 2000 compilation [11], the air-broadened cross-section dataset was expanded to 32 PT combinations (attributed in [11] to a personal communication from Varanasi) covering 180−295 K and 20−760 Torr over the same spectral region, and the linelist was relegated to a supplemental folder. The 32 cross sections can still be found within HITRAN 2016 [14], which also saw the addition of three 760-Torr-N_2-broadened SF_6 spectra (at 278, 298, and 323 K) from the Pacific Northwest National Laboratory (PNNL) IR database [15]. Despite updates to the $^{32}SF_6$ linelist for HITRAN versions 2004 and 2008, this linelist is still located within the supplemental folder for HITRAN 2016 [14] as it is deemed that the cross sections provide a better simulation of atmospheric spectra. These Varanasi cross sections have been extensively used in satellite remote sensing applications, for example MIPAS and ACE-FTS. However, with a minimum air-broadening pressure of ~20 Torr and the presence of sharp Q-branch structure, these cross sections are not the most appropriate for the mid- to upper stratosphere. To resolve this issue, the present work provides new laboratory measurements of air-broadened SF_6 spectra, rectifying issues with the Varanasi dataset, as well as introducing a number of lower pressure measurements over a range of temperatures (pure SF_6 and air-broadened SF_6 at ~7.5 Torr total pressure). A detailed comparison between the previous Varanasi measurements and those presented in the current work are provided in Section 4.

3. New absorption cross sections of pure and air-broadened sulfur hexafluoride

3.1. Experimental

The experimental setup at the Molecular Spectroscopy Facility (MSF), Rutherford Appleton Laboratory (RAL) and the experimental procedures have been described previously, e.g. [16–18]. All spectra were recorded using a Bruker IFS 125HR Fourier transform spectrometer with a coolable 26-cm pathlength absorption cell. FTS instrumental parameters used for the measurements, sample details, and the cell configuration are summarised in Table 1. The sample pressures and temperatures for each air-broadened spectrum, along with their experimental uncertainties and associated spectral resolutions, are listed in Table 2. Additional pure nitrous oxide (N_2O) spectra were recorded at each temperature for the purposes of calibrating the wavenumber scale of the SF_6 cross sections.

3.2. Generation of absorption cross sections

The procedure for generating the absorption cross sections from measured spectra has been reported in detail previously, e.g.

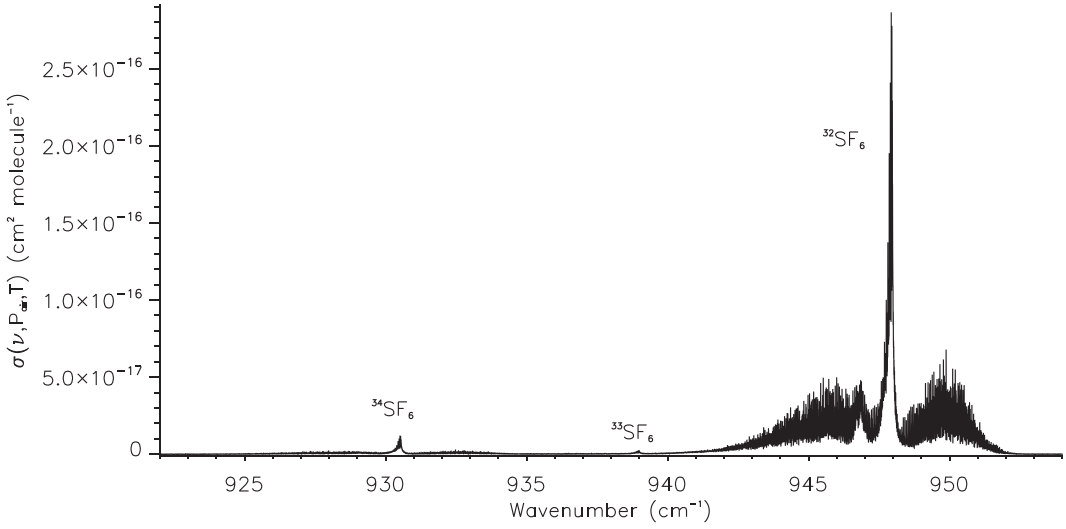

Fig. 1. The absorption cross section of sulfur hexafluoride / dry synthetic air at 189.4 K and 7.50 Torr (this work), showing the ν_3 band for the most abundant $^{32}SF_6$, and minor $^{33}SF_6$ and $^{34}SF_6$ isotopologues.

Table 1
FTS parameters, sample conditions, and cell configuration for all measurements.

Spectrometer	Bruker Optics IFS 125HR
Mid-IR source	Globar
Detector	Mercury cadmium telluride (MCT) D313 [a]
Beam splitter	Potassium bromide (KBr)
Optical filter	~700–1350 cm^{-1} bandpass
Spectral resolution	0.002 to 0.03 cm^{-1}
Aperture size	1.7 to 3.15 mm
Apodisation function	Boxcar
Phase correction	Mertz
SF_6 (CK Gas)	99.9% purity, natural-abundance isotopic mixture
Air zero (BOC Gases)	total hydrocarbons < 3 ppm, H2O < 2 ppm, CO2 < 1 ppm, CO < 1 ppm; used 'as is'
Cell pathlength	26 cm
Cell windows	Potassium bromide (KBr) (wedged)
Pressure gauges	3 MKS-690A Baratrons (1, 10 & 1000 Torr) (±0.05% specified accuracy)
Refrigeration	Julabo F95-SL Ultra-Low Refrigerated Circulator (with ethanol)
Thermometry	4 PRTs, Labfacility IEC 751 Class A
Wavenumber calibration	N_2O

[a] Due to the non-linear response of MCT detectors to the detected radiation, all interferograms were Fourier transformed using Bruker's OPUS software with a non-linearity correction applied.

Table 2
Summary of the sample conditions for all measurements.

Temperature (K)	Initial SF_6 Pressure (Torr)[a]	Total Pressure (Torr)	Spectral resolution (cm^{-1})[b]	Aperture (mm)	Cross section uncertainty (%)
190.1 ± 0.3	0.00572	–	0.0020	1.7	3.8
189.4 ± 0.3	0.01259	7.501 ± 0.003	0.0045	2.5	2.2
189.2 ± 0.5	0.01577	50.40 ± 0.20	0.0150	3.15	2.2
189.2 ± 0.5	0.01682	99.92 ± 0.26	0.0150	3.15	2.2
189.2 ± 0.5	0.01601	201.4 ± 0.2	0.0225	3.15	2.1
202.1 ± 0.3	0.00768	–	0.0020	1.7	3.8
202.1 ± 0.3	0.01283	7.503 ± 0.003	0.0045	2.5	2.2
202.3 ± 0.5	0.01696	51.29 ± 0.09	0.0150	3.15	2.2
202.3 ± 0.5	0.01923	103.1 ± 0.2	0.0150	3.15	2.1
202.4 ± 0.5	0.01975	200.3 ± 0.5	0.0225	3.15	2.2
202.3 ± 0.5	0.02691	299.8 ± 0.5	0.0300	3.15	2.1
216.2 ± 0.3	0.00935	–	0.0020	1.7	3.8
216.4 ± 0.5	0.01277	7.501 ± 0.004	0.0045	2.5	2.2
216.4 ± 0.5	0.02219	50.64 ± 0.06	0.0150	3.15	2.2
216.4 ± 0.5	0.02255	102.0 ± 0.2	0.0150	3.15	2.1
216.5 ± 0.5	0.02658	202.5 ± 0.1	0.0225	3.15	2.1
216.4 ± 0.5	0.02783	360.5 ± 0.4	0.0300	3.15	2.1
232.7 ± 0.4	0.01117	–	0.0020	1.7	3.8
232.5 ± 0.5	0.01749	7.502 ± 0.002	0.0045	2.5	2.2
232.5 ± 0.4	0.02808	49.90 ± 0.03	0.0150	3.15	2.1
232.5 ± 0.4	0.02897	99.81 ± 0.02	0.0150	3.15	2.1
232.5 ± 0.4	0.02952	201.6 ± 0.1	0.0225	3.15	2.1
232.5 ± 0.4	0.04083	404.2 ± 0.1	0.0300	3.15	2.1
252.3 ± 0.5	0.01175	–	0.0020	1.7	3.8
252.3 ± 0.4	0.02442	7.512 ± 0.003	0.0045	2.5	2.2
252.3 ± 0.2	0.04042	50.34 ± 0.02	0.0150	3.15	2.1
252.3 ± 0.2	0.05139	200.8 ± 0.0	0.0225	3.15	2.1
252.3 ± 0.2	0.05103	400.6 ± 0.0	0.0300	3.15	2.1
252.3 ± 0.2	0.05139	600.9 ± 0.2	0.0300	3.15	2.1
273.7 ± 0.3	0.01391	–	0.0020	1.7	3.8
274.0 ± 0.4	0.02956	7.522 ± 0.003	0.0045	2.5	2.2
273.9 ± 0.2	0.06229	209.2 ± 0.0	0.0225	3.15	2.1
273.9 ± 0.2	0.06090	381.3 ± 0.1	0.0300	3.15	2.1
273.9 ± 0.2	0.06364	750.4 ± 0.1	0.0300	3.15	2.1
294.0 ± 0.3	0.01694	–	0.0020	1.7	3.8
293.0 ± 0.1	0.06604	385.0 ± 0.0	0.0300	3.15	2.1
292.9 ± 0.1	0.06804	750.9 ± 0.1	0.0300	3.15	2.1

[a] MKS-690A Baratron readings are specified accurate to ± 0.05%.
[b] Using the Bruker definition of 0.9/MOPD.

[16–18]. The transmittance, $\tau(\upsilon,P_{air},T)$, at wavenumber υ (cm^{-1}), temperature T (K) and synthetic air pressure P_{air}, can be related to the absorption cross section, $\sigma(\upsilon,P_{air},T)$ with units cm^2 $molecule^{-1}$, by

$$\sigma(\nu, P_{air}, T) = \frac{10^4 k_B T}{Pl} \ln \tau(\nu, P_{air}, T) \quad (1)$$

where P is the pressure of the absorbing gas (Pa), l is the optical pathlength (m) and k_B is the Boltzmann constant (= $1.3806488 \times 10^{-23}$ J K^{-1}).

For this work, the absorption cross sections were normalised according to

$$\int_{780\ cm^{-1}}^{1100\ cm^{-1}} \sigma(\nu, P_{air}, T)\partial\nu = 1.9658 \times 10^{-16}\ cm\ molecule^{-1} \quad (2)$$

where the right-hand-side value is the average integrated intensity over the spectral range 780 – 1100 cm^{-1} for two 760-Torr-N_2-broadened SF_6 spectra (at 278 and 298 K) from the Pacific North-

Table 3
Sources of uncertainty in the SF_6 absorption cross sections.

Uncertainty source	Symbol	Maximum uncertainty (1σ)
Temperature	μ_T	0.3%
Pressure	μ_P	0.9%
Photometric uncertainty	μ_{phot}	1.5%
Pathlength	μ_{path}	0.1%
PNNL integrated intensity (780–1100 cm^{-1})	μ_{PNNL}	1.5%
Baseline uncertainty	$\mu_{baseline}$	3.2% (pure) 0.4% (7.5 Torr) 0.2% ($\geq$ 50 Torr)

west National Laboratory (PNNL) IR database [15]. This intensity calibration procedure corrects for problems with SF_6 adsorption in the vacuum line and on the cell walls, with the assumption that the integrated intensity over each band system is independent of temperature. The reader is referred to Ref. 16 for a more complete explanation of the underlying assumption, and references cited within Refs. 17 and 18 for details on previous successful uses of this approach.

3.3. Absorption cross section uncertainties

The wavenumber scale was calibrated using the positions of isolated N_2O absorption lines in the range 1140 to 1320 cm^{-1} from the HITRAN 2016 database [14]. The uncertainty of the wavenumber scale is comparable to the wavenumber uncertainty of the N_2O lines used in the calibration. Although HITRAN uncertainty codes indicate this uncertainty is between 0.001 and 0.0001 cm^{-1}, N_2O line positions from the NIST heterodyne wavenumber calibration tables [19] (accuracy between 0.00005 cm^{-1} and 0.00008 cm^{-1}) agree closely with HITRAN, indicating the uncertainty is actually between 0.0001 and 0.00001 cm^{-1}.

The signal-to-noise ratios (SNRs) for the measured transmittance spectra depend on the spectral resolution / aperture size used; SNR values, calculated using Bruker's OPUS software at ~ 905 cm^{-1} where the transmittance is close to 1, range from 2600 to 3700 for measurements with aperture 3.15 mm and resolutions 0.015 to 0.030 cm^{-1} (samples with total pressure $\geq$ 50 Torr), 920 to 980 for aperture 2.5 mm and resolution 0.0045 cm^{-1} (samples with total pressure ~ 7.5 Torr), and 270 to 410 for aperture 1.7 mm and resolution 0.002 cm^{-1} (samples of pure SF_6). Due to the conversion factor in Eq. (1), which varies between the different measurements, the relative noise for the absorption cross sections differs from that of the original transmittance spectra.

Systematic errors dominate the uncertainty budget of the absorption cross sections. Table 3 lists the principle sources of systematic error and their maximum values; uncertainties in temperature and total pressure are additionally provided in Table 2. Although random, the SNRs of the measured transmittance spectra contribute systematic error to the determination of baseline positions when deriving the cross sections; this contributes systematic error to the normalisation process of Eq. (2), most notably for the pure SF_6 cross sections. Assuming that the systematic errors for these quantities are uncorrelated, the overall systematic error, $\mu_{systematic}$, is determined by adding the contributions in quadrature and taking the square root; this gives a systematic error of 2.1–2.2% (1σ) for the air-broadened and 3.8% (1σ) for the pure SF_6 absorption cross sections.

4. Discussion

This section outlines how the new absorption cross sections improve upon those of Varanasi. A selection of the new cross sections are plotted in Figs. 2 and 3. Fig. 2 shows air-broadened absorption cross sections at a total pressure of ~ 200 Torr for six tem-

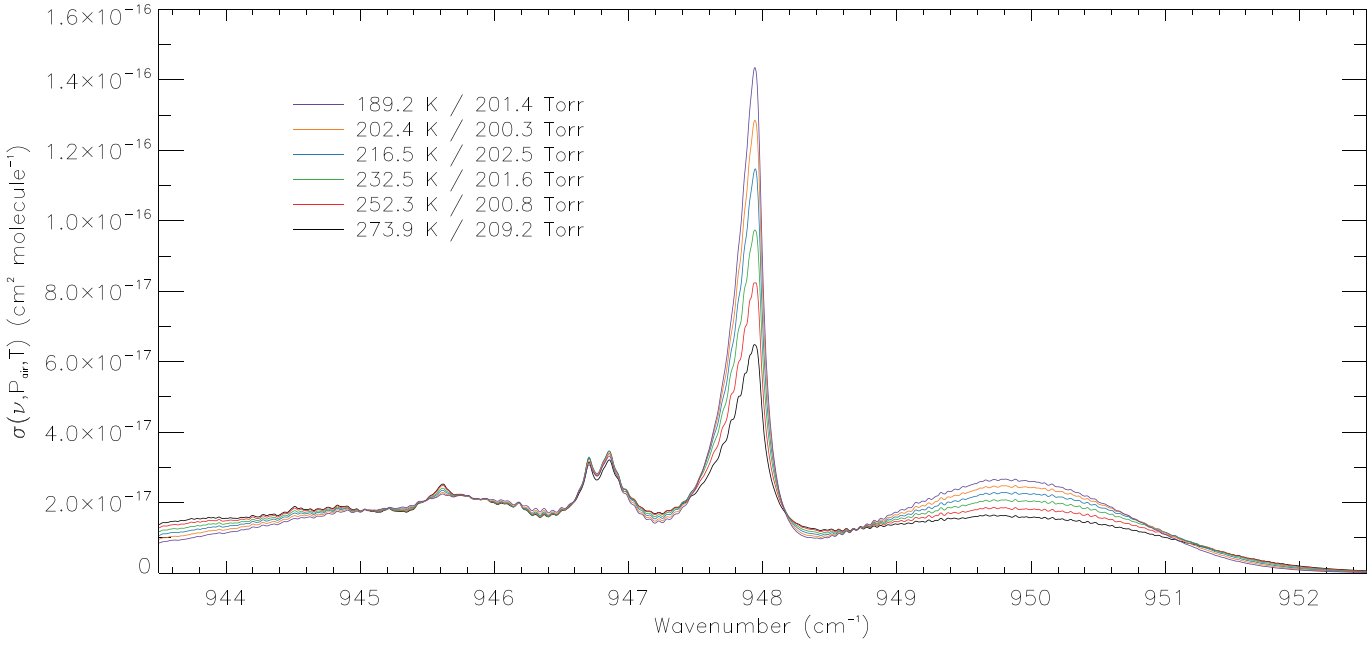

Fig. 2. The absorption cross sections of sulfur hexafluoride / dry synthetic air in the 943.5 – 952.5 cm^{-1} microwindow used for the v4.0 ACE-FTS SF_6 retrieval at a total pressure of ~ 200 Torr over a range of temperatures (189.2, 202.4, 216.5, 232.5, 252.3, and 273.9 K).

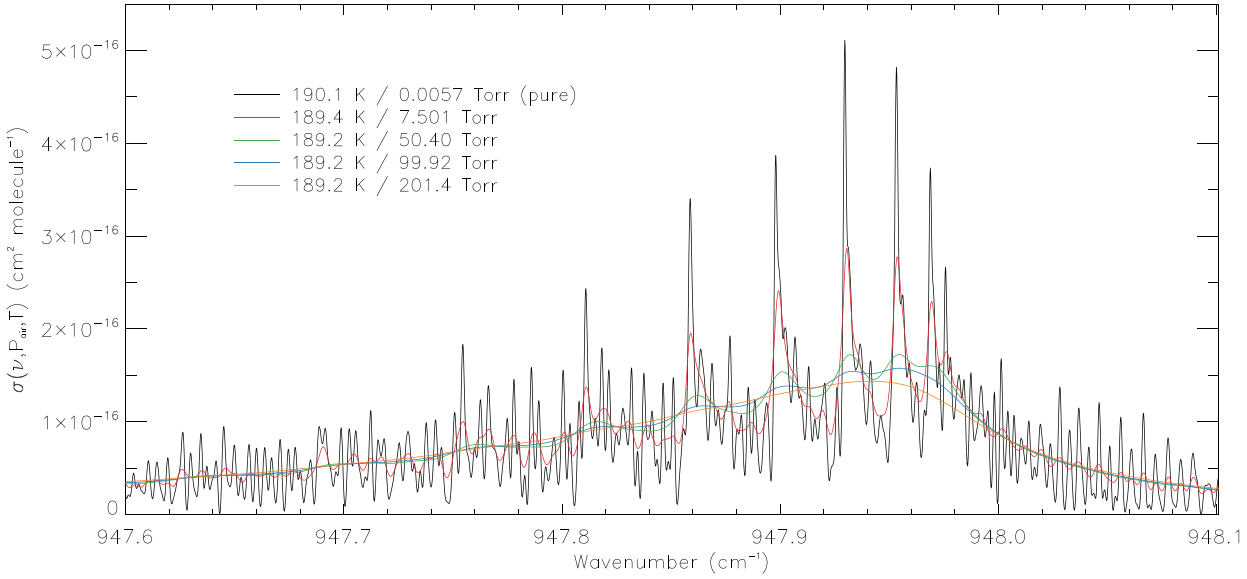

Fig. 3. The absorption cross sections of sulfur hexafluoride / dry synthetic air covering the strongest features of the ν_3 band Q branch ($^{32}SF_6$) at a temperature of ~189 K over a range of pressures (7.501, 50.40, 99.92, and 201.4 Torr); overplotted is the cross section for pure sulfur hexafluoride (~0.0057 Torr) at 190.1 K.

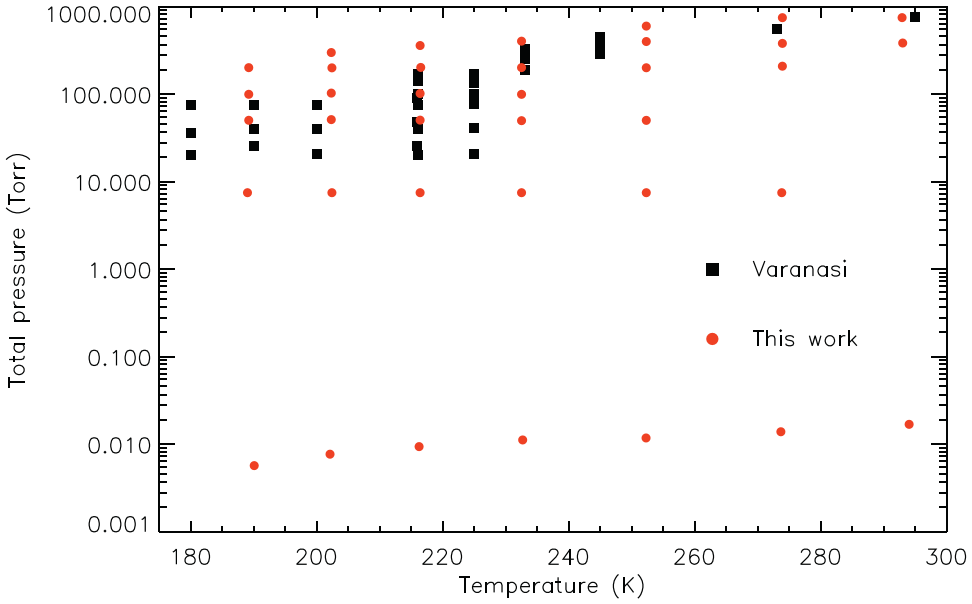

Fig. 4. A graphical representation of the PT coverage for the new sulfur hexafluoride absorption cross section dataset. Note that pressures below 0.02 Torr represent cross sections for pure SF_6, all others are total SF6/air pressures.

peratures over the 943.5 – 952.5 cm^{-1} microwindow used for the v4.0 ACE-FTS SF_6 retrieval. Fig. 3 contains cross sections at ~190 K for five pressures ranging from ~0.0057 Torr (pure) to 201.4 Torr (air-broadened) over the spectral region 947.6 – 948.1 cm^{-1}, which contains the strongest features of the ν_3 band Q branch ($^{32}SF_6$).

As discussed in Section 2, this work extends the range of pressure and temperature combinations for the absorption cross sections for air-broadened (and pure) SF_6; the range was chosen to cover that of ACE-FTS v3.0 data, i.e. conditions from the mid-troposphere (~ 5 km) up to the stratosphere. In particular, the PT coverage has been extended by providing additional high pressure cross sections below 220 K and lower pressure cross sections above 220 K. This can be visualised in Fig. 4, in which temperature is plotted against total pressure (on a logarithmic scale) for each cross section. One major point of difference between datasets is the inclusion of six air-broadened (~7.5 Torr) and seven pure cross sections between 190 and 300 K in the present study; these conditions are crucial in order for atmospheric limb sounders to measure SF_6 profiles accurately at altitudes in the mid/upper stratosphere. Fig. 3 provides an example of the enhanced spectroscopic structure present in low-pressure absorption cross sections at ~190 K (947.6 – 948.1 cm^{-1}). In total, this new cross-section dataset contains 37 different combinations of pressure and temperature (see Table 2).

In addition to a suitable PT coverage, a good absorption cross section dataset requires spectral features that are adequately resolved. In the Varanasi dataset, the spectral resolutions are generally appropriate, however there are three cross sections at 215.9 K and 25.3, 47.6, 90.0 Torr which were derived from spectra recorded at 0.03 cm^{-1} resolution and are very obviously under-resolved. For this work, spectral resolutions were chosen based on the total pressure of the sample, i.e. 0.0045 cm^{-1} for ~7.5 Torr, 0.015 cm^{-1}

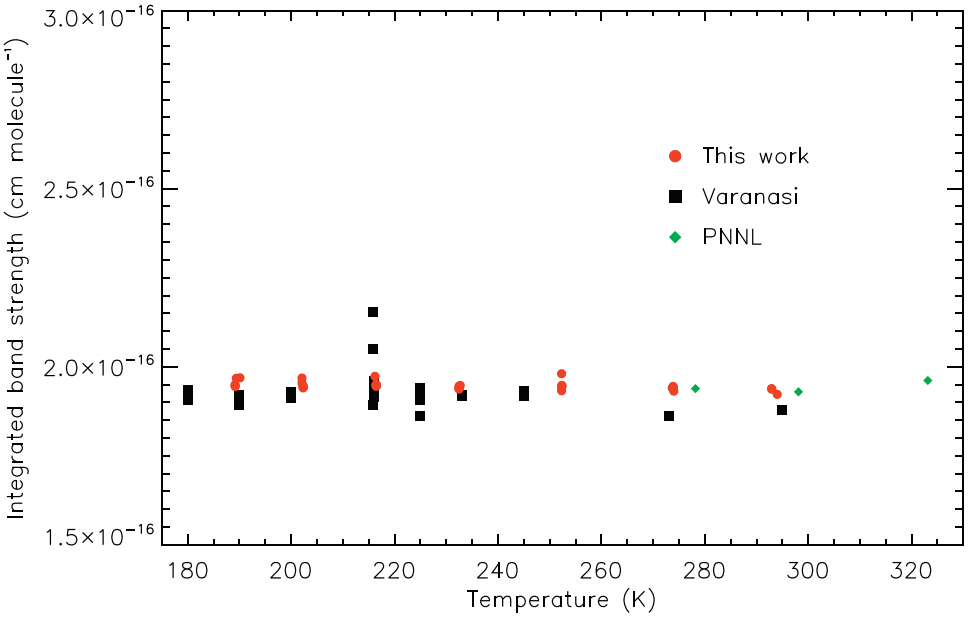

Fig. 5. Integrated band intensity versus temperature for three sulfur hexafluoride cross section datasets (Varanasi, PNNL, and the present work) over the wavenumber range 925 – 955 cm^{-1}.

for ~50 – ~100 Torr, 0.0225 cm^{-1} for ~200 Torr, and 0.03 cm-1 for ~300 Torr and above; for the pure spectra, 0.002 cm^{-1} resolution was used.

The wavenumber scale of the Varanasi cross sections is badly calibrated, if at all. This finding is consistent with previous comparisons between older Varanasi datasets of halogenated species and those derived from more recent measurements, e.g. for CFC-12 [17] and HCFC-22 [18]. With an absolute accuracy in the wavenumber scale of between 0.0001 and 0.00001 cm^{-1} for the new cross sections, the ν_3 band at 948.1 cm^{-1} for the Varanasi data is systematically shifted too low in wavenumber by ~0.004 cm^{-1} (a correction factor of ~ 1.000004).

Unfortunately, the wavenumber range chosen for the Varanasi cross sections (925 – 955 cm^{-1}) cuts off the edge of the ν_3 band, making it difficult to check the veracity of the baselining and compare with the new dataset. Integrated band intensities have been calculated over this wavenumber range (925 – 955 cm^{-1}, i.e. using the range of the Varanasi cross sections) for the PNNL, Varanasi and new cross sections; these are plotted against temperature in Fig. 5. Scatter in the Varanasi integrated band intensities is as high as 15%; the data at ~ 216 K are largely responsible for this, suggesting errors in these measurements. Band intensities for the present work agree very well with those for PNNL, however this is to be expected due to the normalisation procedure. Some of the scatter in the new dataset (this work) can be attributed to cutting off the wavenumber range at 955 cm^{-1}, which slightly reduces the integrated band intensities for high pressure measurements. Despite this, the integrated band intensities of the new cross sections all agree within the quoted experimental error; refer to Table 2.

The SNRs of the new measurements were discussed in Section 3.3. Without the original Varanasi transmittance spectra or information on the experimental mixing ratios, it is difficult to directly compare with the new measurements, however from a visual inspection the new cross sections generally have improved SNR over the range of pressures and temperatures covered by the Varanasi dataset. Additionally, many of the Varanasi cross sections display noticeable channel fringing above the noise level, e.g. peak-to-peak amplitudes in transmittance are over 1% for the cross section at 25.4 Torr and 190.0 K. The new measurements undertaken in the present study use wedged cell windows to prevent reflections along the optical path of the spectrometer.

The new SF_6 absorption cross section dataset will be made available to the community via the HITRAN [14] and GEISA [20] databases, but in the meantime is available electronically from the author.

5. Conclusions

New high-resolution IR absorption cross sections for pure and air-broadened SF_6 have been determined over the spectral range 780 – 1100 cm^{-1}, with estimated systematic uncertainties between 2.1 and 3.8% (1σ). Spectra were recorded at resolutions between 0.002 and 0.03 cm^{-1} (calculated as 0.9/MOPD) over a range of atmospherically relevant temperatures (189 – 294 K) and pressures (up to 751 Torr). These new absorption cross sections improve upon those previously used for the satellite remote sensing of SF_6, and will provide a more accurate basis for retrievals in the future.

Declaration of Competing Interest

The author declares that they have no known competing financial interests or personal relationships that could have appeared to influence the work reported in this paper.

CRediT authorship contribution statement

Jeremy J. Harrison: Conceptualization, Methodology, Software, Validation, Formal analysis, Investigation, Writing - original draft, Writing - review & editing, Visualization, Supervision, Project administration.

Acknowledgements

This study was funded as part of the UK Research and Innovation Natural Environment Research Council's support of the National Centre for Earth Observation, contract number PR140015. The author wishes to thank R.A. McPheat, R.G. Williams, and R.A. Brownsword for providing technical support during the measurements.

References

[1] IPCC. In: Stocker TF, Qin D, Plattner G-K, Tignor M, Allen SK, Boschung J, et al., editors. Climate Change 2013: the Physical Science Basis. Contribution of Working Group I to the Fifth Assessment Report of the Intergovernmental Panel on Climate Change. Cambridge, United Kingdom and New York, NY, USA: Cambridge University Press; 2013. p. 1535.

[2] Harnisch J, Eisenhauer A. Natural CF_4 and SF_6 on Earth. Geophys Res Lett 1998;25:2401–4. doi:10.1029/98GL01779.

[3] Engel A, Rigby M, Burkholder JB, Fernandez RP, Froidevaux L, Hall BD, et al. Update on Ozone-Depleting Substances (ODSs) and Other Gases of Interest to the Montreal Protocol, Chapter 1 in Scientific Assessment of Ozone Depletion: 2018 Global Ozone Research and Monitoring Project–Report, 58. Geneva, Switzerland: World Meteorological Organization; 2018.

[4] Ravishankara AR, Solomon S, Turnipseed AA, Warren RF. Atmospheric lifetimes of long-lived halogenated species. Science 1993;259(5092):194–9. doi:10.1126/science.259.5092.194.

[5] Kovács T, Feng W, Totterdill A, Plane JMC, Dhomse S, Gómez-Martín JC, Stiller GP, Haenel FJ, Smith C, Forster PM, García RR, Marsh DR, Chipperfield MP. Determination of the atmospheric lifetime and global warming potential of sulfur hexafluoride using a three-dimensional model. Atmos Chem Phys 2017;17:883–98. doi:10.5194/acp-17-883-2017.

[6] Ray EA, Moore FL, Elkins JW, Rosenlof KH, Laube JC, Röckmann T, et al. Quantification of the SF_6 lifetime based on mesospheric loss measured in the stratospheric polar vortex. J Geophys Res Atmos 2017;122:4626–38. doi:10.1002/2016JD026198.

[7] Haenel FJ, Stiller GP, von Clarmann T, Funke B, Eckert E, Glatthor N, Grabowski U, Kellmann S, Kiefer M, Linden A, Reddmann T. Reassessment of MIPAS age of air trends and variability. Atmos Chem Phys 2015;15:13161–76. doi:10.5194/acp-15-13161-2015.

[8] Brown AT, Chipperfield MP, Boone C, Wilson C, Walker KA, Bernath PF. Trends in atmospheric halogen containing gases since 2004. J Quant Spectrosc Radiat Transf 2011;112:2552–66. doi:10.1016/j.jqsrt.2011.07.005.

[9] Faye M, Boudon V, Loëte M, Roy P, Manceron L. The high overtone and combination levels of SF_6 revisited at Doppler-limited resolution: a global effective rovibrational model for highly excited vibrational states. J Quant Spectrosc Radiat Transf 2017;190:38–47. doi:10.1016/j.jqsrt.2017.01.006.

[10] Varanasi P, Li Z, Nemtchinov V, Cherukuri A. Spectral absorption-coefficient data on HCFC-22 and SF_6 for remote-sensing applications. J Quant Spectrosc Radiat Transf 1994;52:323–32.

[11] Rothman LS, Barbe A, Benner DC, Brown LR, Camy-Peyret C, Carleer MR, Chance K, Clerbaux C, Dana V, Devi VM, Fayt A, Flaud J-M, Gamache RR, Goldman A, Jacquemart D, Jucks KW, Lafferty WJ, Mandin J-Y, Massie ST, Nemtchinov V, Newnham DA, Perrin A, Rinsland CP, Schroeder J, Smith KM, Smith MAH, Tang K, Toth RA, Vander Auwera J, Varanasi P, Yoshino K. The HITRAN molecular spectroscopic database: edition of 2000 including updates through 2001. J Quant Spectrosc Radiat Transf 2003;82:5–44.

[12] Rothman LS, Gamache RR, Tipping RH, Rinsland CP, Smith MAH, Benner DC, Devi VM, Flaud J-M, Camy-Peyret C, Perrin A, Goldman A, Massie ST, Brown LR, Toth RA. The HITRAN molecular database: editions of 1991 and 1992. J Quant Spectrosc Radiat Transf 1992;48:469–507.

[13] Rothman LS, Rinsland CP, Goldman A, Massie ST, Edwards DP, Flaud J-M, Perrin A, Camy-Peyret C, Dana V, Mandin J-Y, Schroeder J, Mccann A, Gamache RR, Wattson RB, Yoshino K, Chance KV, Jucks KW, Brown LR, Nemtchinov V, Varanasi P. The HITRAN molecular spectroscopic database and hawks (HITRAN atmospheric workstation): 1996 edition. J Quant Spectrosc Radiat Transf 1998;60:665–710.

[14] Gordon IE, Rothman LS, Hill C, Kochanov RV, Tan Y, Bernath PF, Birk M, Boudon V, Campargue A, Chance KV, Drouin BJ, Flaud J-M, Gamache RR, Hodges JT, Jacquemart D, Perevalov VI, Perrin A, Shine KP, Smith M-AH, Tennyson J, Toon GC, Tran H, Tyuterev G, Barbe A, Császár AG, Devi VM, Furtenbacher T, Harrison JJ, Hartmann J-M, Jolly A, Johnson TJ, Karman T, Kleiner I, Kyuberis AA, Loos J, Lyulin OM, Massie ST, Mikhailenko SN, Moazzen-Ahmadi N, Müller HSP, Naumenko OV, Nikitin AV, Polyansky OL, Rey M, Rotger M, Sharpe SW, Sung K, Starikova E, Tashkun SA, Vander Auwera J, Wagner G, Wilzewski J, Wcisło P, Yu S, Zak EJ. The HITRAN2016 molecular spectroscopic database. J Quant Spectrosc Radiat Transf 2017;203:3–69. doi:10.1016/j.jqsrt.2017.06.038.

[15] Sharpe SW, Johnson TJ, Sams RL, Chu PM, Rhoderick GC, Johnson PA. Gas-phase databases for quantitative infrared spectroscopy. Appl Spectrosc 2004;58:1452–61.

[16] Harrison JJ, Allen NDC, Bernath PF. Infrared absorption cross sections for ethane (C_2H_6) in the 3 μm region. J Quant Spectrosc Radiat Transf 2010;111:357–63. doi:10.1016/j.jqsrt.2009.09.010.

[17] Harrison JJ. New and improved infrared absorption cross sections for dichlorodifluoromethane (CFC-12). Atmos Meas Tech 2015;8:3197–207. doi:10.5194/amt-8-3197-2015.

[18] Harrison JJ. New and improved infrared absorption cross sections for chlorodifluoromethane (HCFC-22). Atmos Meas Tech 2016;9:2593–601. doi:10.5194/amt-9-2593-2016.

[19] Maki AG, Wells JS. Wavenumber calibration tables from heterodyne frequency measurements. NIST special publication 821, National Institute of Standards and Technology. Gaithersburg 1991.

[20] Jacquinet-Husson N, Armante R, Scott NA, Chédin A, Crépeau L, Boutammine C, Bouhdaoui A, Crevoisier C, Capelle V, Boonne C, Poulet-Crovisier N, Barbe A, Benner DC, Boudon V, Brown LR, Buldyreva J, Campargue A, Coudert LH, Devi VM, Down MJ, Drouin BJ, Fayt A, Fittschen C, Flaud J-M, Gamache RR, Harrison JJ, Hill C, Hodnebrog Ø, Hu S-M, Jacquemart D, Jolly A, Jiménez E, Lavrentieva NN, Liu A-W, Lodi L, Lyulin OM, Massie ST, Mikhailenko S, Müller HSP, Naumenko OV, Nikitin A, Nielsen CJ, Orphal J, Perevalov VI, Perrin A, Polovtseva E, Predoi-Cross A, Rotger M, Ruth AA, Yu SS, Sung K, Tashkun SA, Tennyson J, Tyuterev VIG, Vander Auwera J, Voronin BA, Makie A. The 2015 edition of the GEISA spectroscopic database. J Mol Spectrosc 2016;327:31–72. doi:10.1016/j.jms.2016.06.007.